



Computer Method of Determining the Yield Surface of Variable Structure of Heterogeneous Materials Based on the Statistical Evaluation of Their Elastic Characteristics

Mariya Shapovalova^(✉)  and Oleksii Vodka 

Department of Dynamics and Strength of Machines, National Technical University,
Kharkiv Polytechnic Institute, Kharkiv, Ukraine

Abstract. The study of the material microstructure allows obtaining information about the state of the part without additional tests and full-scale experiments. The paper offers computer methods for constructing parametric, statistically equivalent models of cast iron microstructure with the inclusion of spheroidal graphite. The studied material has a transient microstructure that exhibits variability at various material points. To analyze the unsteadiness of deformations, the Monte Carlo method is used. A finite element model is constructed to find the elastic characteristics of the material. The stress state is considered based on plane models. Numerical experiments are carried out for various concentrations of inclusions. The results obtained for the elastic constants are statistically averaged, and the dependences of the Poisson's ratio, the moduli of elasticity, and the shear moduli on the concentration of the inclusions are established. For veracity assessment, the values obtained are compared with those obtained using the mixture rule. The results of the application of the rule confirm the correctness of the built models. The yield surfaces are found, going beyond the surface indicates the appearance of plastic strains in the material.

Keywords: High strength cast iron · Microstructure · Finite element method · Material properties · Yield surface

1 Introduction

The use of composite materials requires a detailed study of their internal structure. To understand the behavior of the structure during operation, it is necessary to know the mechanical properties of the material and the boundary stress values at which failure-free operation is possible. Assessing the internal structure of the sample at the micro-level, the method of analyzing the microstructure image is widely used. High-strength cast iron has found application in mechanical engineering [31, 32]. It is used in critical assemblies, such as gears, gearboxes, suspension arms, etc. A feature of such cast iron is its relatively simple microstructure. The microstructure of cast iron with the inclusion of spherical graphite is represented in Fig. 1.

Such approaches to the analysis of the material macrostructure are known in the literature. Experimental [1–6] or direct research. They require the creation of samples and the experiment conducting. Work is known where the influence of the microstructure on crack development [1], phase composition [2], the hardness of the test sample [6].

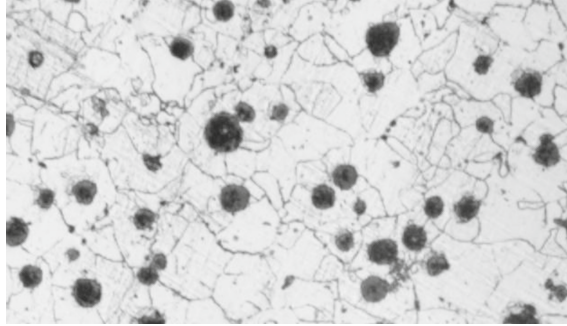


Fig. 1. The microstructure of high-strength cast iron [25]

The second group of studies [7–13], combines the application of computer vision technology. Image pattern recognition is used to classify the structure [7, 10]; assessment of the number of defects [8]; segmentation of complex microstructures [11], finding the particle sizes and their distribution on the plane, predicting the properties of the material by the image of its microstructure [12, 13]. Other works [14–18] propose modeling the studied microstructure by the finite element method.

This paper proposes to create a methodology for studying microstructure without additional full-scale experiment, to use the advantages of computer vision for microstructure recognition. The proposed technique relies on the generation of statistically equivalent microstructure geometry, independent of the particular image. The studied material is characterized by a transition microstructure. Such a structure exhibits variability at various points on the surface. For analysis, a method of averaging material characteristics is used. The position and orientation of graphite inclusions on the ferrite plane are randomly generated by a numerical method. The obtained statistical data allows describing of the variability microstructure influence on the sample's mechanical properties. Including analysis of the stress-strain state and equivalent elastic constants by the finite element method. Elements of the same technics could be found in [26–30].

2 Objectives

As the initial data in the work, images of the microstructure of cast iron are taken (Fig. 1). It is assumed that the structure of cast iron is modeled synthetically, based on actual images of its microstructure. It is necessary to take into account the possibility of a random position of inclusions on the plane and consider the possibility of varying their concentration depending on the size of graphite. To determine the elastic properties of the investigated material by modeling a finite elemental model. To obtain the characteristics

of the elastic moduli, shear moduli, and Poisson's ratio as a function of the concentration of inclusions. Find the invariants of the elastic moduli. They provide information on the elastic characteristics of the material. Build the yield surface, which ensures the absence of plastic strains.

3 Image Processing and Generation of the Statistically Equivalent Artificial Microstructure

Image processing and artificial microstructure generation of high-strength cast iron have been implemented in previous works [19, 20]. The generation of the statistically equivalent microstructure of cast iron is possible by establishing the dependence of the size of inclusions on their concentration. For each concentration case, data have been obtained on the number and size of graphite inclusions on the plane. According to mathematical expectation data, the variance of the radii inclusions, their number per area, the function of the dependence of the size of the inclusions on the concentration have been obtained by (1):

$$\begin{aligned} M[R] &= 18.308 \cdot (\psi - 0.048)^{0.123}; \\ \sqrt{D[R]} &= 9.683 \cdot (\psi - 0.045)^{0.314}. \end{aligned} \quad (1)$$

The nature of inclusions obeys the normal distribution law of a random variable. Each radius of graphite inclusions is randomly generated while their total area is less than the required concentration. By concentration (ψ) is meant the ratio of the area of inclusions to the area of the sample, which varies in the range of [0.054..0.3]. The position of radii centers on the plane of the simulated cast iron microstructure also occurs randomly and implemented by a uniform quantity distribution function. The result of the artificial generation of the microstructure is shown in Fig. 2.

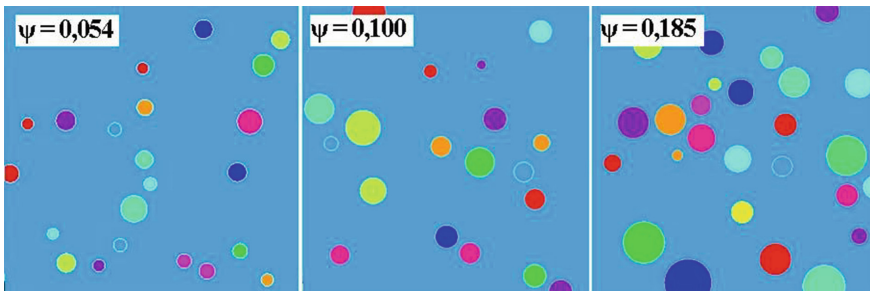


Fig. 2. Artificially generated microstructure with an appropriate concentration of inclusions

4 Finite Element Model

The construction of the finite elemental model is based on the geometry (Fig. 2) obtained after the artificial generation of the cast iron microstructure. To create the mesh grid,

a two-dimensional 8-node finite element with two degrees of freedom in each node is used. Typical meshing is shown in Fig. 3. For calculations, it is assumed that ferrite is an isotropic material, in Table 1 shows its mechanical properties, and graphite – has a hexagonal structure of the crystal lattice, the corresponding elastic constants are given in Table 2.

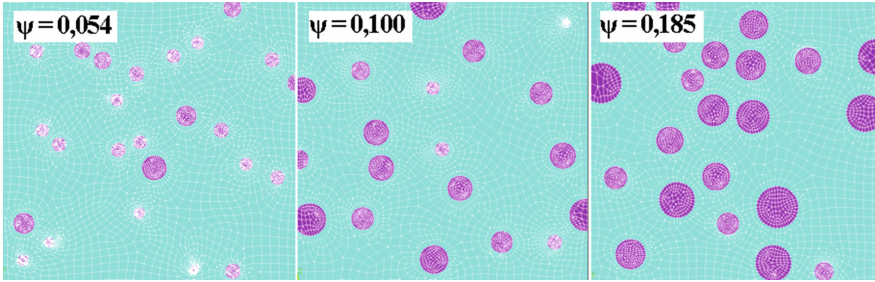


Fig. 3. The typical meshing of cast iron microstructure

Table 1. Properties of ferrite material

E, GPa	N	Yield strength, MPa
210	0.3	125

Table 2. Properties of graphite material

E _x , E _z , GPa	E _y , GPa	ν _{xy}	ν _{yz}	ν _{xz}	G _{xy} , G _{xz} , GPa	G _{yz} , GPa	Yield strength, MPa	
							Compression	Tensile
1025	36	0.34	0.012	0.16	0.18	4.35	480	100

5 Homogenization Procedure and Elastic Constant Determination

Based on the macro level, structural elements are considered homogeneous anisotropic materials with averaged elastic characteristics. Hooke’s law for anisotropic material can be written for the case of general anisotropy by (2):

$$\langle \varepsilon_{ij} \rangle = A_{ijkl} \langle \sigma_{kl} \rangle, (i, j, k, l = 1, 2, 3), \tag{2}$$

where A_{ijkl} – elastic constants of equivalent homogeneous material;

$\langle \sigma_{ij} \rangle, \langle \varepsilon_{ij} \rangle$ – the mean strain and strain tensors averaged as the integral by volume (3).

$$\langle \sigma_{ij} \rangle = \frac{1}{V} \int_V \sigma_{ij} dV; \langle \varepsilon_{ij} \rangle = \frac{1}{V} \int_V \varepsilon_{ij} dV. \tag{3}$$

Using the Voigt notation [23] and the above concepts are introduced, the 4th rank symmetric tensor from Eq. (2) can be written using a quadratic matrix. In an arbitrarily chosen orthogonal coordinate system, Hooke’s law can be represented in a matrix form (4) [17].

$$\begin{bmatrix} \langle \varepsilon_x \rangle \\ \langle \varepsilon_y \rangle \\ \langle \varepsilon_z \rangle \\ \langle \gamma_{yz} \rangle \\ \langle \gamma_{zx} \rangle \\ \langle \gamma_{xy} \rangle \end{bmatrix} = \begin{bmatrix} a_{11} & a_{12} & a_{13} & a_{14} & a_{15} & a_{16} \\ a_{21} & a_{22} & a_{23} & a_{24} & a_{25} & a_{26} \\ a_{31} & a_{32} & a_{33} & a_{34} & a_{35} & a_{36} \\ a_{41} & a_{42} & a_{43} & a_{44} & a_{45} & a_{46} \\ a_{51} & a_{52} & a_{53} & a_{54} & a_{55} & a_{56} \\ a_{61} & a_{62} & a_{63} & a_{64} & a_{65} & a_{66} \end{bmatrix} \times \begin{bmatrix} \langle \sigma_x \rangle \\ \langle \sigma_y \rangle \\ \langle \sigma_z \rangle \\ \langle \tau_{yz} \rangle \\ \langle \tau_{zx} \rangle \\ \langle \tau_{xy} \rangle \end{bmatrix}, \tag{4}$$

where a_{ik} elastic constants; in the general case, the number of independent elastic constants is 21, according to symmetry $a_{ik} = a_{ki}$.

As a test sample, plane artificially modeled images of cast iron microstructure are taken, therefore it’s correct to calculate the stress based on plane models. Equation (4) for the case of a plane stress state takes the form (5):

$$\begin{bmatrix} \langle \varepsilon_x \rangle \\ \langle \varepsilon_y \rangle \\ \langle \gamma_{xy} \rangle \end{bmatrix} = \begin{bmatrix} a_{11} & a_{12} & a_{16} \\ a_{21} & a_{22} & a_{26} \\ a_{61} & a_{62} & a_{66} \end{bmatrix} \times \begin{bmatrix} \langle \sigma_x \rangle \\ \langle \sigma_y \rangle \\ \langle \tau_{xy} \rangle \end{bmatrix}. \tag{5}$$

In technical application, such notation (6) are often used [21]:

$$\begin{aligned} a_{11} &= \frac{1}{E_x}; a_{22} = \frac{1}{E_y}; a_{66} = \frac{1}{G_{xy}}; a_{12} = -\frac{\nu_{xy}}{E_x}; a_{21} = -\frac{\nu_{yx}}{E_y}; \\ a_{16} &= \frac{\eta_{x,xy}}{G_{xy}}; a_{26} = \frac{\eta_{y,xy}}{G_{xy}}; a_{61} = \frac{\eta_{xy,x}}{E_x}; a_{62} = \frac{\eta_{xy,y}}{E_y}, \end{aligned} \tag{6}$$

where $E_x, E_y, \nu_{xy}, \nu_{yx}$ – Young’s moduli; ν_{xy}, ν_{yx} – Poisson’s ratio; G_{xy} – shear module; $\eta_{xy,x}, \eta_{xy,y}$ – the 1st order coefficients of interaction that characterize the displacement in the directions parallel to the coordinate axes under the action of normal stresses; $\eta_{x,xy}, \eta_{y,xy}$ – the 2nd order interaction coefficients that characterize the elongation in directions parallel to the coordinate axes caused by the shear stresses.

Then Hooke’s law (5), taking into account the notation (6), will take the form (7). Based on the statement about the symmetry of the matrix, have six independent elastic constants, and three are linearly dependent on the diagonal constants determined from Eqs. (8):

$$\begin{bmatrix} \langle \varepsilon_x \rangle \\ \langle \varepsilon_y \rangle \\ \langle \gamma_{xy} \rangle \end{bmatrix} = \begin{bmatrix} \frac{1}{E_x} & -\frac{\nu_{xy}}{E_x} & \frac{\eta_{x,xy}}{G_{xy}} \\ -\frac{\nu_{yx}}{E_y} & \frac{1}{E_y} & \frac{\eta_{y,xy}}{G_{xy}} \\ \frac{\eta_{xy,x}}{E_x} & \frac{\eta_{xy,y}}{E_y} & \frac{1}{G_{xy}} \end{bmatrix} \times \begin{bmatrix} \langle \sigma_x \rangle \\ \langle \sigma_y \rangle \\ \langle \tau_{xy} \rangle \end{bmatrix}. \tag{7}$$

$$E_x \nu_{yx} = E_y \nu_{xy}; E_x \eta_{x,xy} = G_{xy} \eta_{xy,x}; E_y \eta_{y,xy} = G_{xy} \eta_{xy,y}. \tag{8}$$

To obtain the matrix it’s necessary to find all the constants four numerical experiments have to be performed. The load diagram of the model, the results of which allows creating a system of linear algebraic equations for the Poisson’s ratio, elastic and shear moduli represented in Fig. 4.

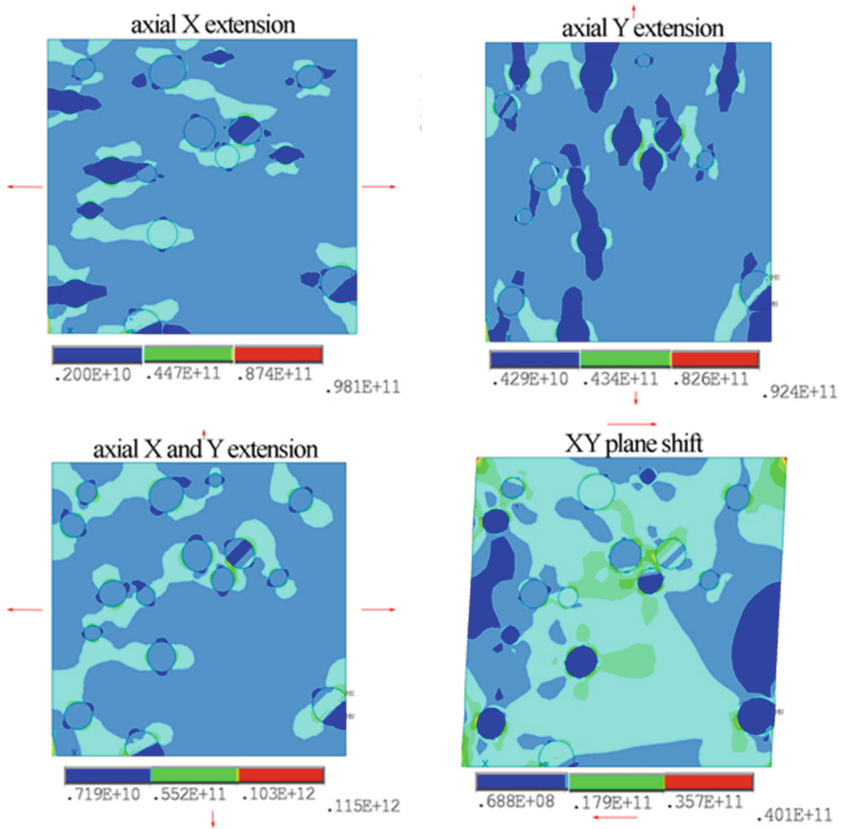


Fig. 4. Von Mises equivalent stresses under different types of loads

6 The Results of Elastic Constant Conclusion

The results of the stress-strain state of the microstructure of cast iron with the inclusion of spherical graphite in four types of load are represented in Fig. 4. Considering the orientation of inclusions to be arbitrary, it is necessary to conduct a series of numerical experiments to obtain elastic constants.

To determine the elastic constants, the Monte Carlo method is used. According to this method, the position and orientation of inclusions on the plane are set randomly. For each concentration, 200 Monte Carlo algorithm interventions are performed. The results obtained for elastic constants are statistically averaged, and their dependence on the concentration of inclusions is established (Fig. 5). The dependence (9) is taken as the confidence interval for the calculated data, which for the normal distribution of a random variable corresponds to 99.73% of the probability of the results being in this region.

$$\alpha_{\text{int}} = M \pm 3 \cdot \sqrt{D}, \quad (9)$$

where M and D – mathematical expectation and variance of the corresponding elastic constants.

The averaged results for 200 numerical experiments for the elastic moduli, Poisson’s ratio, shear moduli, and the 1st and 2nd order coefficients of the mutual influence of stresses for 17 concentrations of graphite inclusions are given in Table 3.

Table 3. Elastic characteristics of the studied material

ψ	E_x, GPa	E_y, GPa	G_{xy}, GPa	$\nu_{xy}, \times 10^{-2}$	$\nu_{yx}, \times 10^{-2}$	$\eta_{x,xy}, \times 10^{-3}$	$\eta_{y,xy}, \times 10^{-3}$	$\eta_{xy,x}, \times 10^{-3}$	$\eta_{xy,y}, \times 10^{-3}$
0.054	195.58	196.13	74.54	31.56	31.65	-0.70	0.31	-1.87	0.85
0.057	195.70	195.59	74.14	31.54	31.52	1.28	-1.04	3.32	-2.76
0.060	194.32	194.63	73.81	31.73	31.78	0.15	-0.48	0.59	-1.52
0.065	193.37	193.68	73.05	31.75	31.81	1.36	-0.11	3.59	-0.27
0.070	192.70	193.13	72.24	31.71	31.78	1.57	-1.24	4.32	-3.24
0.075	190.87	191.63	72.04	31.98	32.11	-0.21	2.44	-0.45	6.55
0.080	190.02	190.50	71.19	32.07	32.15	-1.35	-1.14	-3.60	-2.98
0.085	189.56	189.72	70.71	32.07	32.11	-1.98	0.17	-5.23	0.18
0.090	187.94	188.33	70.64	32.32	32.38	0.65	-0.71	1.90	-2.20
0.100	186.16	186.16	68.93	32.53	32.53	-1.64	0.49	-4.95	1.78
0.135	178.43	178.75	65.59	33.27	33.35	-1.83	2.40	-5.25	6.52
0.150	174.98	174.17	65.06	34.19	34.03	0.76	2.12	2.89	3.89
0.170	170.40	168.81	63.64	34.99	34.68	-2.81	5.41	-6.61	14.32
0.185	166.62	166.56	62.19	35.21	35.18	1.69	-2.32	5.09	-7.02
0.200	163.98	163.95	60.76	35.46	35.46	-0.98	3.55	-3.24	9.11
0.250	155.47	156.33	56.25	36.13	36.34	-0.40	-3.51	-0.07	-10.15
0.300	147.21	144.73	53.40	38.09	37.53	1.13	2.68	2.67	6.62

To assess the veracity, the results obtained have been compared with the results obtained using the mixture rule (10). This approach makes it possible to estimate the upper and lower boundaries of the elastic moduli. These estimates correspond to parallel and perpendicular structural elements (Fig. 6). An analysis of the results shows that the mathematical expectation of the equivalent moduli of elasticity is between the upper and lower bounds of the estimate according to the rule of the mixture, which confirms the correctness of the constructed models. However, from it is seen that the upper boundary of the confidence interval exceeds the upper estimate of the elastic moduli. This is because the rule of the mixture does not take into account the random orientation of the principal axes of the graphite crystals, and a comparison is possible only by average values. This is also since the real properties of graphite are much more complicated than isotropic, which provides for the rule of the mixture.

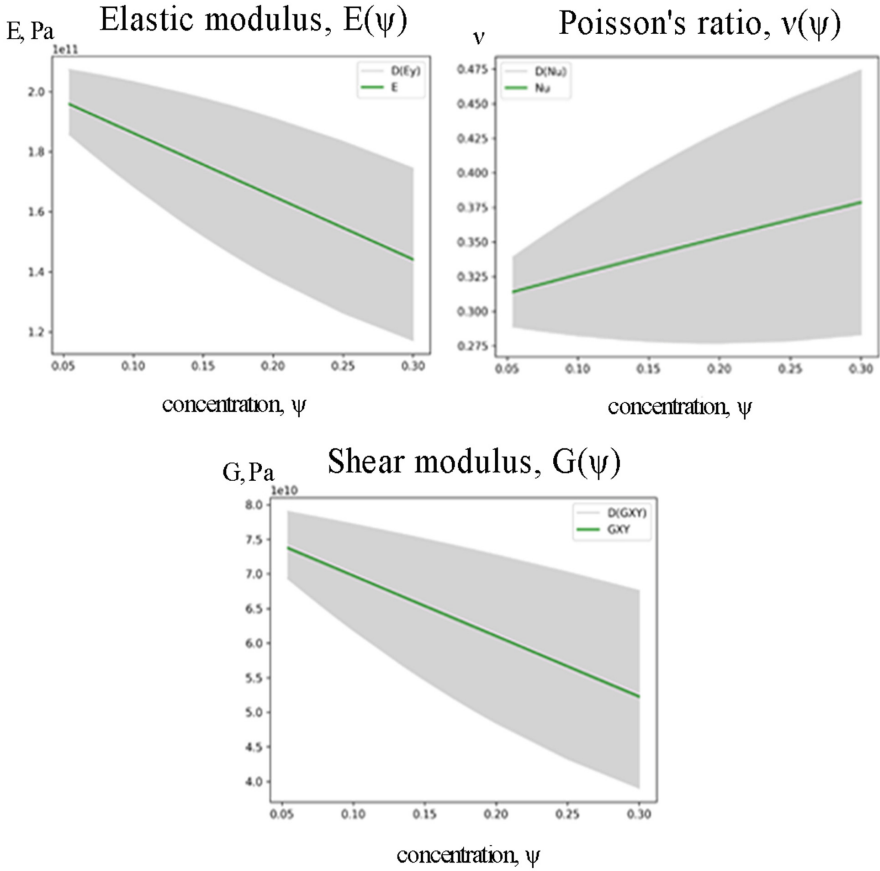


Fig. 5. The dependence of the elastic characteristics of the material on the concentration of inclusions

$$E_{\max} = \psi \cdot E_g + (1 - \psi) \cdot E_f; E_{\min} = \left(\frac{\psi}{E_g} + \frac{1 - \psi}{E_f} \right)^{-1}, \quad (10)$$

where, ψ – concentration in the range [0.054, 0.300]; E_g – graphite elastic moduli; E_f – ferrite elastic moduli.

On the other hand, in the literature [22], the problems of finding the invariants of the elastic moduli tensor are often considered. Such invariants have a mechanical meaning and provide information on the elastic properties of the material under study. The found invariants of the elastic moduli provide information on the properties of the material and require the establishment of a smaller number of independent constants.

To find the corresponding invariants, it is necessary to introduce the concepts: eigenvalues – λ , and Eigen tensor of the second rank – q_{ij} . Then, for a plane stress state, the tensor takes the form (11):

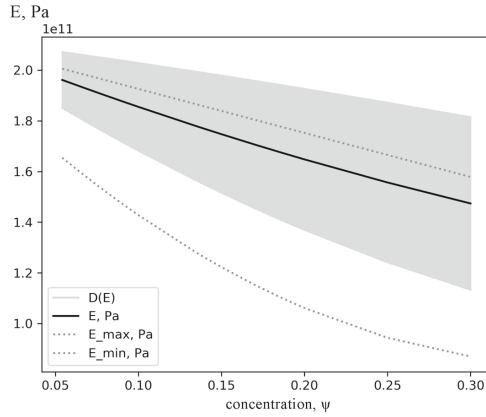


Fig. 6. The upper and lower boundaries of the elastic moduli of the generated microstructure

$$A_{ij} \cdot q_j = \lambda \cdot q_i, (i, j = 1, 2, 3). \tag{11}$$

$$\begin{cases} (A_{11} - \lambda) \cdot q_1 + A_{12} \cdot q_2 + A_{13} \cdot q_3 = 0 \\ A_{21} \cdot q_1 + (A_{22} - \lambda) \cdot q_2 + A_{23} \cdot q_3 = 0 \\ A_{31} \cdot q_1 + A_{32} \cdot q_2 + (A_{33} - \lambda) \cdot q_3 = 0 \end{cases} \tag{12}$$

The system of linear Eqs. (12) gives three orthonormal Eigen tensors: $q_i^{(1)}, q_i^{(2)}, q_i^{(3)}$. Stresses and strains are represented by the expansion along with the basis of intrinsic tensors (13):

$$\begin{aligned} \sigma_i &= k_1^{(\sigma)} \cdot q_i^{(1)} + k_2^{(\sigma)} \cdot q_i^{(2)} + k_3^{(\sigma)} \cdot q_i^{(3)} \Rightarrow \sigma_i^*; \\ \varepsilon_i &= k_1^{(\varepsilon)} \cdot q_i^{(1)} + k_2^{(\varepsilon)} \cdot q_i^{(2)} + k_3^{(\varepsilon)} \cdot q_i^{(3)} \Rightarrow \varepsilon_i^*; \\ k_1^{(\sigma)} &= \sigma_i \cdot q_i^{(1)}; k_2^{(\sigma)} = \sigma_i \cdot q_i^{(2)}; k_3^{(\sigma)} = \sigma_i \cdot q_i^{(3)}; \\ k_1^{(\varepsilon)} &= \sigma_i \cdot q_i^{(1)}; k_2^{(\varepsilon)} = \sigma_i \cdot q_i^{(2)}; k_3^{(\varepsilon)} = \sigma_i \cdot q_i^{(3)}. \end{aligned} \tag{13}$$

Given Eq. (13), Hooke’s law in matrix form has a diagonal form (14), the elastic moduli are given in three positive definite eigenvalues $\lambda_i > 0, (i = 1, 2, 3)$:

$$\begin{bmatrix} \langle \sigma_i^* \rangle \\ \langle \sigma_i^* \rangle \\ \langle \sigma_i^* \rangle \end{bmatrix} = \begin{bmatrix} \lambda_1 & 0 & 0 \\ 0 & \lambda_2 & 0 \\ 0 & 0 & \lambda_3 \end{bmatrix} \times \begin{bmatrix} \langle \varepsilon_i^* \rangle \\ \langle \varepsilon_i^* \rangle \\ \langle \varepsilon_i^* \rangle \end{bmatrix}. \tag{14}$$

Using the linear algebra library `numpy.linalg`, the eigenvalue and the right eigenvectors of the square array for the elastic moduli are calculated. The results of mathematical expectation and variance for three invariants of the elastic moduli and six elastic constants for various concentrations of inclusions are shown in Table 4, and such dependence is graphically shown in Fig. 7.

Table 4. Statistical data of the invariants of the elastic moduli

Ψ	$M[\lambda_1], \times 10^{11}$	$D[\lambda_1], \times 10^{11}$	$M[\lambda_2], \times 10^{10}$	$D[\lambda_2], \times 10^9$	$M[\lambda_3], \times 10^9$	$D[\lambda_3], \times 10^9$
0.054	2.86	1.49	7.45	0.53	1.74	1.20
0.057	2.86	1.49	7.41	0.64	2.19	1.61
0.060	2.85	1.48	7.38	0.75	2.53	1.61
0.065	2.84	1.47	7.30	1.09	3.15	1.86
0.070	2.83	1.47	7.22	1.08	3.02	2.15
0.075	2.82	1.45	7.20	1.19	3.13	2.07
0.080	2.81	1.44	7.11	1.12	3.55	2.20
0.085	2.80	1.44	7.06	1.31	3.83	2.49
0.090	2.79	1.42	7.05	1.42	3.61	2.35
0.100	2.76	1.40	6.90	1.61	4.07	2.63
0.135	2.69	1.34	6.54	2.26	4.88	3.18
0.150	2.66	1.31	6.49	2.56	5.57	3.84
0.170	2.61	1.26	6.34	2.97	5.34	3.20
0.185	2.58	1.24	6.19	3.08	5.61	4.10
0.200	2.55	1.22	6.05	3.06	4.99	3.58
0.250	2.46	1.15	5.59	3.55	7.29	4.04
0.300	2.36	1.07	5.30	4.05	6.89	4.95

7 The Yield Surface Calculation

One of the tasks of materials engineering is to establish the loading conditions that cause plastic deformation. This is important to determine the load combination which leads to a transition from the elastic to the plastic state. To find «safe» loading which is not lead to plastic deformation.

In the case of uniaxial loading, this task is not particularly difficult. It is enough to have a relation between stress and strain. Such data can be obtained from experiments on simple tension and compression. However, for materials that are in conditions of two and three-dimensional stress states, everything is not so clear. In such situations, predicting the appearance of plasticity requires additional information.

In the case of a three-dimensional stress state, determining the yield surface is a difficult task. This is due to several technical difficulties caused on the one hand by the complexity of the experimental environment, and on the other hand, by the huge number of samples that need to be tested. This problem is especially acute for composite and heterogeneous materials. To solve this problem, computer simulation methods are used.

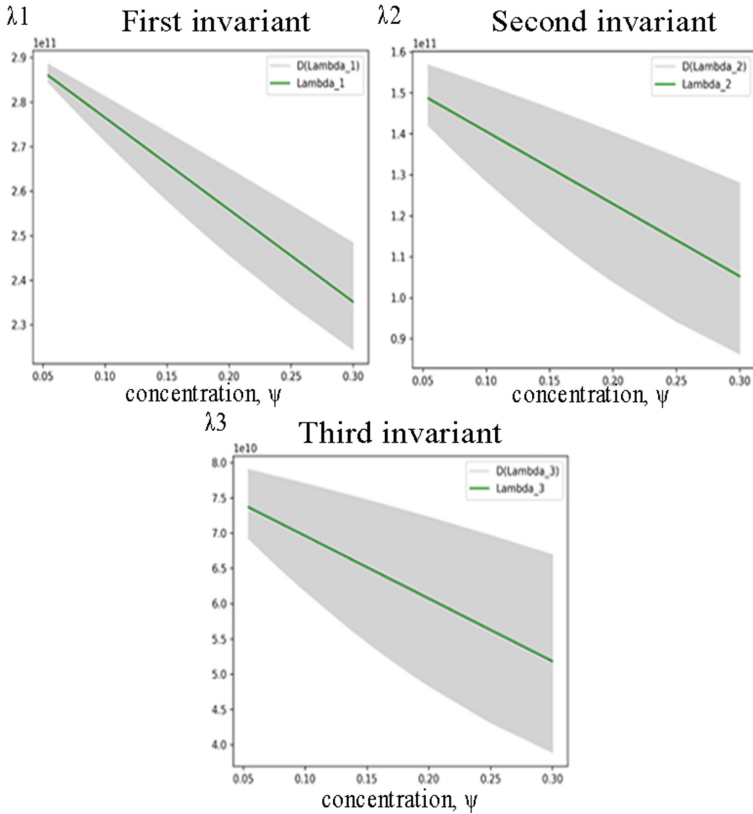
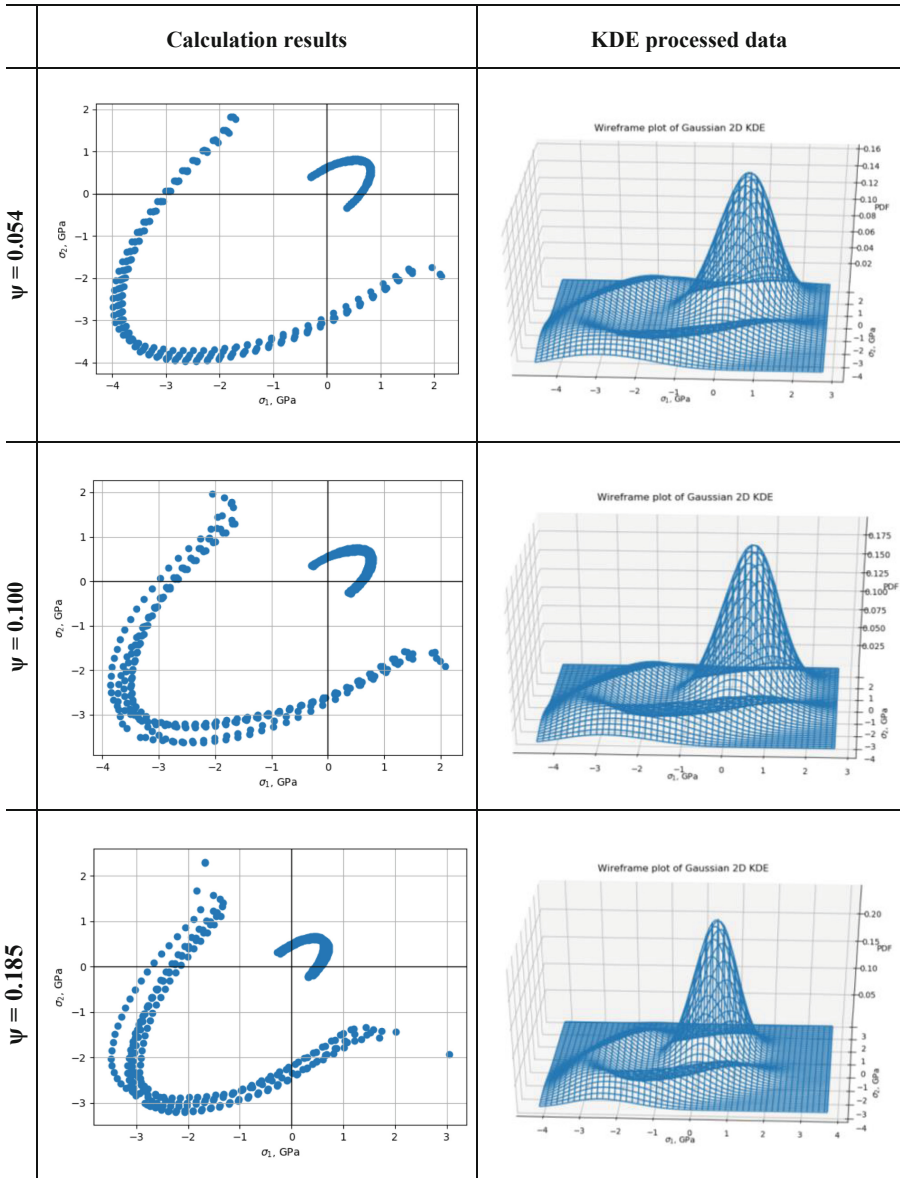


Fig. 7. The dependence of the invariants of the elasticity moduli on the concentration of inclusions

Computer modeling uses yield hypotheses in complex loading conditions [24]. All hypotheses are based on the assumption that the yield of material in a multidimensional stressed state occurs when the value is reached or exceeded the specific value obtained from a simple uniaxial test.

The finding of the yield surface in this work is based on the hypothesis of the specific energy of shaping (the Huber – Mises – Genki hypothesis) [24]. According to the hypothesis, plastic strains of a sample in a complex stress state occurs when the specific formation energy becomes equal to or exceeds the specific formation energy of the material under the action of a uniaxial stress state.

For the microstructure which is consists of two types of materials (ferrite and graphite), the maximum stresses for each phase are found. For graphite, the tensile and compressive strengths differ significantly, therefore, separately for each type of stress state, the ratios maximum stresses to the corresponding allowable tensile strength are found. The yield surface is determined by the ratio of the principal stresses to the safety factor. The calculation result for some concentrations of graphite inclusions in the structure of ferrite is presented graphically in Table 5.

Table 5. Yield surface for different concentration of inclusions

The first column in Table 5 contains some concentrations of graphite inclusions. The second column contains the calculation results presented as a set of points where the abscissa axis is σ_1 and the ordinate is σ_2 . These quantities are the maximum allowable values of the principal stresses for ferrite and graphite materials respectively.

Kernel density estimation (KDE) is a way to estimate the probability density function (PDF) of a random variable in a non-parametric way. In the third column of Table 5 presented a PDF of the principals stress values obtained during calculations. Yield surface for different concentration of inclusions built with a library of statistical functions `scipy.stats` using `gaussian_kde` method to calculate the estimator bandwidth.

8 Conclusions

The paper discusses an algorithm for studying the elastic mechanical properties of cast iron. The elemental analysis of the created structural model is completed, the obtained formulas for determining the elastic moduli, Poisson's ratio, and shear moduli are completed. The analysis of the dependence of elastic characteristics on the content of graphite inclusions is carried out. To evaluate the results, the mixture rule is applied to the averaged elastic moduli. The results of numerical modeling showed a good ratio of the calculated values of the Poisson's ratio, elastic moduli, and shear with reference data. On the other hand, the maximum allowable values of the principal stresses for ferrite and graphite materials are calculated. According to the received data yield surfaces for various concentrations of inclusions have been found and constructed. Going beyond the surface indicates the appearance of plastic strains in the part.

Acknowledgment. This work has been supported by the Ministry of Education and Science of Ukraine in the framework of the realization of the research projects: «Development of methods for mathematical modeling of the behavior of new and composite materials aims to structural elements lifetime estimation and prediction of engineering designs reliability» (State Reg. Num. 0117U004969), and «Development of methods of computational intelligence in problems of synthesis of characteristics of responsible elements, increase of reliability and efficiency of innovative equipment» (State Reg. Num. 0121U100730).

References

1. Sikoraab, P., Elrahmanac, M., Chunga, S.-Y., Cendrowskid, K., Mijowskad, E., Stephana, D.: Mechanical and microstructural properties of cement pastes containing carbon nanotubes and carbon nanotube-silica core-shell structures, exposed to elevated temperature. *Cement Concr. Compos.* **95**, 193–204 (2019). <https://doi.org/10.1016/j.cemconcomp.2018.11.006>
2. Salinas, A., Celentano, D., Carvajal, L., Artigas, A., Monsalve, A.: Microstructure-based constitutive modelling of low-alloy multiphase TRIP steels. *Metals* **9**(2), 250 (2019). <https://doi.org/10.3390/met9020250>
3. Xu, H., Zhu, M., Marcicki, J., Yang, X.: Mechanical modeling of battery separator based on microstructure image analysis and stochastic characterization. *J. Power Sources* **345**, 137–145 (2017). <https://doi.org/10.1016/j.jpowsour.2017.02.002>
4. Son, S., et al.: Investigation of the microstructure of laser-arc hybrid welded boron steel. *JOM* **70**(8), 1548–1553 (2018). <https://doi.org/10.1007/s11837-018-2876-2>
5. Zhang, Y., et al.: Influence of graphite morphology on phase, microstructure, and properties of hot dipping and diffusion aluminizing coating on flake/spheroidal graphite cast iron. *Metals* **9**(4), 450 (2019). <https://doi.org/10.3390/met9040450>

6. Ramakrishnan, G., Dinda, P.: Microstructure and mechanical properties of direct laser metal deposited Haynes 282 superalloy. *Mater. Sci. Eng.* **748**(4), 347–356 (2019). <https://doi.org/10.1016/j.msea.2019.01.101>
7. DeCost, B., Holm, E.: A computer vision approach for automated analysis and classification of microstructural image data. *Comput. Mater. Sci.* **110**, 126–133 (2015). <https://doi.org/10.1016/j.commatsci.2015.08.011>
8. Pereira, R.F., da Silva Filho, V.E.R., Moura, L.B., Kumar, N.A., de Alexandria, A.R., de Albuquerque, V.H.C.: Automatic quantification of spheroidal graphite nodules using computer vision techniques. *J. Supercomput.* **76**(2), 1212–1225 (2018). <https://doi.org/10.1007/s11227-018-2579-z>
9. Campbell, A., Murray, P., Yakushina, E., Marshall, S., Ion, W.: New methods for automatic quantification of microstructural features using digital image processing. *Mater. Des.* **141**, 395–406 (2018). <https://doi.org/10.1016/j.matdes.2017.12.049>
10. Kwon, O., et al.: A deep neural network for classification of melt-pool images in metal additive manufacturing. *J. Intell. Manuf.* **31**(2), 375–386 (2018). <https://doi.org/10.1007/s10845-018-1451-6>
11. DeCost, B., Lei, B., Francis, T., Holm, E.: High throughput quantitative metallography for complex microstructures using deep learning: a case study in ultrahigh carbon steel. *Microsc. Microanal.* **25**(1), 21–29 (2019). <https://doi.org/10.1017/S1431927618015635>
12. Fragassa, C., Babic, M., Bergmann, C., Minak, G.: Predicting the tensile behavior of cast alloys by a pattern recognition analysis on experimental data. *Metals* **9**(5), 557 (2019). <https://doi.org/10.3390/met9050557>
13. Shapovalova, M., Vodka, O.: Image microstructure estimation algorithm of heterogeneous materials for identification their chemical composition. In: IEEE 2nd Ukraine Conference on Electrical and Computer Engineering (UKRCON), Institute of Electrical and Electronics Engineers Inc., Ukraine, Lviv pp. 975–979 (2019). <https://doi.org/10.1109/UKRCON.2019.8879861>
14. Hua, F., Yang, Y., Guo, D., Tong, W., Hu, Z.: Cailiao Kexue Yu Jishu Elasto-plastic FEM analysis of residual stress in spun tube. *J. Mater. Sci. Technol.* **20**, 379–382 (2004)
15. Seriacopi, V., Fukumasu, N., Souza, R., Machado, I.: Finite element analysis of the effects of thermo-mechanical loadings on a tool steel microstructure. *Eng. Fail. Anal.* **97**, 383–398 (2019). <https://doi.org/10.1016/j.engfailanal.2019.01.006>
16. Park, H., Jung, J., Kim, H.: Three-dimensional microstructure modeling of particulate composites using statistical synthetic structure and its thermo-mechanical finite element analysis. *Comput. Mater. Sci.* **126**, 265–271 (2017). <https://doi.org/10.1016/j.commatsci.2016.09.033>
17. Fischer, C., Reichenbacher, A., Metzger, M., Schweizer, C.: Computational assessment of the microstructure-dependent thermomechanical behaviour of AlSi12CuNiMg-T7—methods and microstructure-based finite element analyses. In: Naumenko, K., Krüger, M. (eds.) *Advances in Mechanics of High-Temperature Materials*. ASM, vol. 117, pp. 35–56. Springer, Cham (2020). https://doi.org/10.1007/978-3-030-23869-8_2
18. Vodka, O.: Processing microsection images to determine elastic characteristics of cast iron. IEEE Ukraine SYW-2018 Congress. Student, Young Professional and Women in Engineering, Kyiv, Ukraine (2018)
19. Shapovalovam, M., Vodka, O.: Computer methods for constructing parametric statistically equivalent models of high-strength cast iron microstructure to analyze its elastic characteristics. *Notes of the Tavrida National University V.I. Vernadsky. Series: Technical Sciences*, vol. 30(69), 6, pp. 179–187. (in Ukrainian) (2019). <https://doi.org/10.32838/2663-5941/2019.6-1/33>
20. Shapovalova, M., Vodka, O.: Computer methods for modeling the synthetic structure of cast iron for statistical evaluation of its mechanical properties and strength characteristics. BNTU Minsk: 277–284 ISSN (online): 2310-7405 (2020). (in Russian)

21. Ambatsumian, S.: Theory of Anisotropic Plates. Nayka. Moscow (1967). 268 p. (in Russian)
22. Ostrosablin, N.: About the invariants of the fourth-rank tensor of elastic moduli. Sib. Journ. Industr. Mach. **1**(1), 155–163 (1998). (in Russian)
23. Annin, B., Ostrosablin, N.: Anisotropy of the elastic properties of materials. Appl. Mech. Tech. Physic. **49**(6), 131–151 (2008). (in Russian)
24. Beliaev, N.: Strength of materials. Science, Chap. (ed.) Physical and Mathematical Literature (1965). 856 p. (in Russian)
25. GOST 3443–87: Castings of Cast Iron of Various Shapes of Graphite. Methods for determining the structure (ISO 945–75*). [Instead of GOST 3443–77]. M.: Standardinform. (2005). (in Russian)
26. Kudii, D., Khrypunov, M., Zaitsev, R., Khrypunova, A.: Physical and technological foundations of the chloride treatment of cadmium telluride layers for thin-film photoelectric converters. J. Nano. Electron. Phys. **10**(3), 03007 (2018). [https://doi.org/10.21272/jnep.10\(3\).03007](https://doi.org/10.21272/jnep.10(3).03007)
27. Zaitsev, R., Kirichenko, M., Khrypunov, G., Prokopenko, D., Zaitseva, L.: Hybrid solar generating module development for high-efficiency solar energy station. J. Nano. Electron. Phys. **10**(6), 06017 (2018). [https://doi.org/10.21272/jnep.10\(6\).06017](https://doi.org/10.21272/jnep.10(6).06017)
28. Avdieieva, O., Usatyi, O., Vodka, O.: Development of the typical design of the high-pressure stage of a steam turbine. In: Ivanov, V., Pavlenko, I., Liaposhchenko, O., Machado, J., Edl, M. (eds.) DSMIE 2020. LNME, pp. 271–281. Springer, Cham (2020). https://doi.org/10.1007/978-3-030-50491-5_26
29. Lytvynenko, O., Tarasov, O., Mykhailova, I., Avdieieva, O.: Possibility of using liquid-metals for gas turbine cooling system. In: Ivanov, V., Pavlenko, I., Liaposhchenko, O., Machado, J., Edl, M. (eds.) DSMIE 2020. LNME, pp. 312–321. Springer, Cham (2020). https://doi.org/10.1007/978-3-030-50491-5_30
30. Shapovalova, M., Vodka, O.: A data-driven approach to the prediction of spheroidal graphite cast iron yield surface probability characteristics. In: Nechyporuk, M., Pavlikov, V., Kritskiy, D. (eds.) ICTM 2020. LNNS, vol. 188, pp. 565–576. Springer, Cham (2021). https://doi.org/10.1007/978-3-030-66717-7_48
31. Kelin, A., Larin, O., Naryzhna, R., Trubayev, O., Vodka, O., Shapovalova, M.: Mathematical modelling of residual lifetime of pumping units of electric power stations. In: Nechyporuk, M., Pavlikov, V., Kritskiy, D. (eds.) Integrated Computer Technologies in Mechanical Engineering. AISC, vol. 1113, pp. 271–288. Springer, Cham (2020). https://doi.org/10.1007/978-3-030-37618-5_24
32. Kelin, A., Larin, O., Naryzhna, R., Trubayev, O., Vodka, O., Shapovalova, M.: Estimation of residual life-time of pumping units of electric power stations. In: IEEE 14th International Conference on Computer Sciences and Information Technologies (CSIT), Lviv, Ukraine. 1, 153–159 (2019). <https://doi.org/10.1109/STC-CSIT.2019.8929748>